Holographic elements for modulation transfer function testing of detector arrays

Alfred D. Ducharme
Glenn D. Boreman, MEMBER SPIE
University of Central Florida
Center for Research and Education in Optics and Lasers (CREOL)
Department of Electrical Engineering
Orlando, Florida 32816
E-mail: gdb@infrared.creol.ucf.edu

Abstract. A holographic technique is presented that increases the flux-transfer efficiency of laser speckle generation by a factor of 100 over the integrating sphere method. This makes a wider range of low-power lasers usable for the speckle MTF test method, and increases the number of wavelengths at which the test can be applied.

Subject terms: modulation transfer function measurements; detector arrays; holograms; CCD focal-plane array.

Optical Engineering 34(8), 2455–2458 (August 1995).

1 Introduction

We have previously demonstrated the measurement of the modulation transfer function (MTF) of detector arrays using laser speckle with narrowband spatial-frequency content.[1] An integrating sphere[2] produces this speckle accurately and conveniently. However, to produce detectable speckle patterns over the spatial-frequency range of interest, input laser-flux requirements are typically on the order of 200 mW. The holographic technique described here uses less power by approximately a factor of 100, making the speckle MTF method practical for lower power lasers.

We show that the holographic technique produces speckle with negligible distortion as compared to the direct integrating-sphere approach (rms error less than 2%). The advantages of the method are the same as those presented in Ref. 1. The speckle provides an inherent averaging over the position of the test target with respect to the rows and columns of the detector array. The random nature of the speckle makes the MTF measurement procedure shift-invariant. This relaxes alignment tolerances compared to shift-variant methods[1] while preserving measurement accuracy. Results of various MTF measurement methods agreed within a few percent rms error.[1] The advantage of the holographic approach is the enhanced flux-transfer efficiency.

2 Hologram Recording

Figure 1 is a schematic of an optical setup consisting of a reference wave and an object wave generated with an integrating sphere and two-slit aperture. The majority of the laser power is directed into the integrating sphere using a 95 : 5 beam splitter. This initial beam ratio is needed because the sphere absorbs much of the power directed into its input port. The absorption occurs because the initial flux undergoes many internal reflections before exiting through the output port. The throughput of a sphere with no baffles may be determined theoretically using[3]

$$\tau = \frac{\phi_e}{\phi_i} = \frac{\rho f_e}{1-\rho(1-f_j)} , \tag{1}$$

where ϕ_e is the flux exiting the output port, ϕ_i is the flux entering the sphere, f_e is the ratio of output-port area to total sphere area, and f_j is the ratio of the total port area to total sphere area. Evaluating Eq. (1) for a 2.54-cm-diam sphere with two 4-mm-diam ports and reflectance ρ equal to 0.984 shows that a sphere without baffles has a throughput of 21.6%. The sphere used in this experiment has an additional 6-mm-diam disk baffle, which eliminates radiation passing directly from the input port to the output port. The actual throughput of this integrating sphere (without the two-slit aperture) was measured using a large-area photodetector to be 9.7%.

The measured throughput of the integrating sphere may be used to calculate the power on the hologram. After the 10-mW laser source is divided with the 95 : 5 beam splitter, 9.5 mW enters the integrating sphere. After the integrating sphere absorbs 90.3% of this power, 0.92 mW exits through the output port and is defined as ϕ_e. Assuming Lambertian radiation, the radiance at the output port, L_s, may be expressed as

$$L_s = \frac{\phi_e}{\pi(\pi\, r_e^2)} , \tag{2}$$

where $\pi\, r_e^2$ is the area of the output port. A two-slit aperture is placed at the output port to create the desired pattern. The flux on the hologram placed z (see Fig. 1) from the two-slit aperture is

Paper 08104 received Oct. 6, 1994; revised manuscript received Feb. 11, 1995; accepted for publication Feb. 14, 1995.

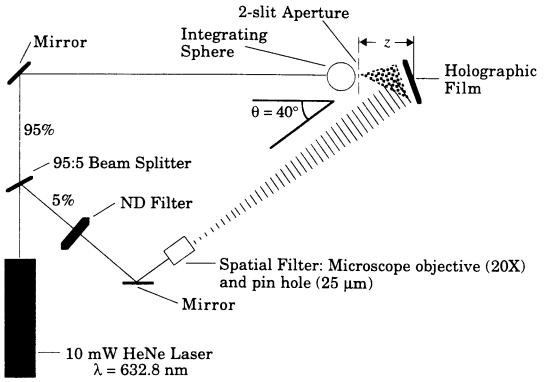

Fig. 1 Optical setup for recording hologram.

$$\phi_{\text{hologram}} = \frac{L_s A_{\text{aperture}} A_{\text{hologram}}}{z^2} \quad . \tag{3}$$

Substituting Eq. (2) into Eq. (3) yields

$$\phi_{\text{hologram}} = \frac{\phi_e A_{\text{aperture}} A_{\text{hologram}}}{\pi(\pi\, r_e^2) z^2} \quad . \tag{4}$$

Calculation of Eq. (4) with $z = 7.5$ cm, $A_{\text{aperture}} = 0.00516$ cm^2, $A_{\text{hologram}} = 1$ cm^2, $r_e = 0.2$ cm, and $\phi_e = 0.92$ mW yields $\phi_{\text{hologram}} = 0.1$ μW.

The amplitude of the interference at the plane of the hologram is maximized when the reference-to-object-beam ratio is 1 : 1. A large-area photodetector was placed at the plane of the hologram to determine the power provided by each beam. The power from the two-slit aperture was measured at the plane of the hologram with a large-area photodetector to be 0.1 μW. The power in the reference beam was then adjusted with a neutral-density (ND) filter, until it also provided 0.1 μW.

The angle θ between the object and reference beams determines the spatial frequency ζ of the fringes recorded in the film emulsion. The relationship between ζ and θ is

$$\zeta = \frac{2}{\lambda} \sin\frac{\theta}{2} \quad . \tag{5}$$

Using a large angle, the integrating sphere can be placed close to the holographic film and the reference beam propagates to the film unobstructed. The largest angle is determined from the maximum resolution (1500 cycles/mm) of the Kodak SO-253 film. We set θ to produce 1125 cycles/mm, yielding

$$1125 = \frac{2}{\lambda} \sin\frac{\theta}{2} \quad . \tag{6}$$

The angle θ was found to be 40 deg, assuming $\lambda = 632.8$ nm.

At 632.8 nm, the film has a sensitivity of 1.12 μJ/cm^2, and produces a hologram with an optical density of 1.0 before bleaching, which optimizes diffraction efficiency during playback. The exposure time is obtained by dividing the film sensitivity by the incident irradiance on the film. A typical input irradiance was 0.2 μW/cm^2, yielding an exposure time of approximately 6.

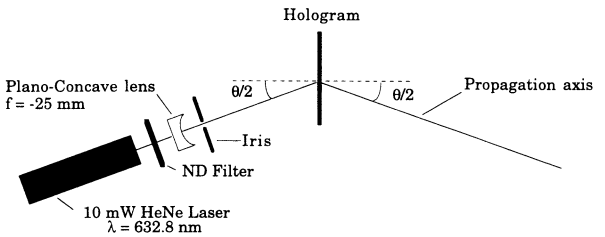

Fig. 2 Optical setup for playback of hologram.

After exposure of the hologram, the film is developed using a 5-min bath of Kodak D-19 developer, a water rinse, and a final 2-min bath in Kodak fixer solution. This process produces an amplitude-type hologram. The amplitude hologram is transformed to a phase hologram, which has a higher diffraction efficiency, by using a modified R-10 bleach solution[4] between the developer and fixer steps.

3 Hologram Playback

The playback system shown in Fig. 2 will provide a speckle pattern that scales with distance from the holographic film. A plano-concave lens reilluminates the hologram with a divergent plane wave, which produces a real image of the two-slit aperture to form about 7.5 cm beyond the hologram. The speckle pattern then scales from this image plane with distance according to

$$\xi = \frac{L}{\lambda z} \quad , \tag{7}$$

where L is the slit spacing in the aperture, ξ is the spatial frequency, and z is the distance from the image of the two-slit aperture to the observation plane. The reilluminating wave is incident on the hologram at the same angle used during recording. This ensures the highest possible diffraction efficiency, according to the Bragg condition.[5]

The speckle pattern propagates in the direction along the axis shown in Fig. 2. Speckle images are recorded at various distances along this axis to measure the detector-array MTF. An example of a holographically produced midfrequency narrowband speckle pattern is shown in Fig. 3(a). The speckle pattern in Fig. 3(b) is a typical narrowband laser speckle pattern produced directly with an integrating sphere and a two-slit aperture. The holographic system faithfully reproduces the original test target.

4 Flux Requirements

Figure 4(a) shows the distribution of power among the beams that are produced during playback of the hologram. These percentages were measured by focusing each beam separately onto a large-area photodetector and dividing by the measured input power. The total power in the speckle pattern produced by the hologram, using a 10-mW laser, is 120 μW. For the same 10-mW laser, the total power in the speckle pattern [see Fig. 4(b)] produced with the integrating sphere is 40 μW. From this comparison it is evident that the hologram is initially three times more flux-efficient than the integrating sphere and two-slit aperture.

A greater improvement in flux efficiency for the hologram is seen when the flux is measured at increasing distances from

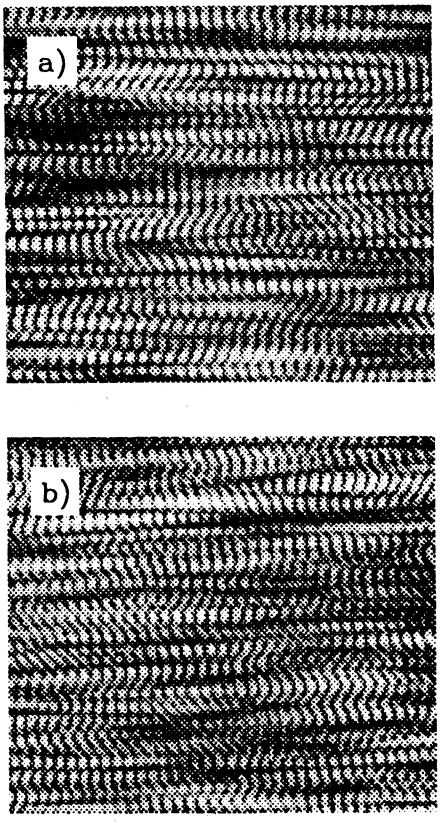

Fig. 3 Examples of narrowband laser speckle produced (a) holographically and (b) with an integrating sphere and a two-slit aperture.

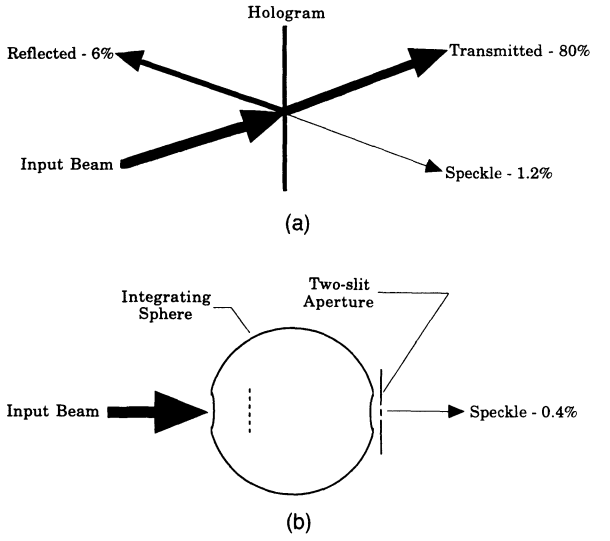

Fig. 4 Breakdown of power consumption for (a) hologram playback and (b) integrating sphere and two-slit aperture.

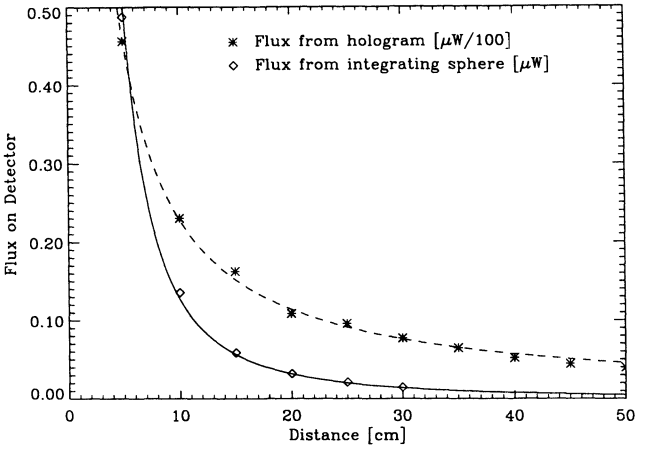

Fig. 5 Flux on 1-cm^2 photodetector for integrating sphere and hologram, as a function of distance.

each system. Figure 5 is a plot of the flux on a 1-cm^2 photodetector as a function of distance (5 cm$<z<$50 cm) for each system. The distance is measured from the two-slit aperture for the integrating-sphere system and from the image of the two-slit aperture for the hologram system. Equation (4) shows that the flux on the photodetector will decrease as $1/z^2$. This falloff is shown as the solid line, with good agreement. The speckle pattern produced by the hologram is more collimated, and as a result the flux on the photodetector is empirically seen to fall off more slowly, approximately as $1/z$. The dashed line is a $1/z$ fit for the data produced by the holographic system. The most important feature in Fig. 5 is that flux in the speckle pattern produced with the holographic system is at least 100 times greater at each distance shown. Thus, the hologram can be used for MTF testing using a lower-power laser (2 mW) than would be required for direct use with the integrating sphere (200 mW).

5 Verification of Instrumental MTF

The MTF of the instrument, including both the recording and playback of the hologram, must be characterized to assure that MTFs measured with the hologram are accurate. To measure the instrument MTF, we used a slant-slit aperture[1] that produces a speckle pattern with a flat power-spectral density (PSD) over an extended region of spatial frequency. This aperture was placed in the recording setup shown in Fig. 1. A hologram of the resulting speckle pattern was recorded and then played back in the setup shown in Fig. 2.

An image of the resulting speckle pattern was recorded at a distance z and processed to yield the PSD of the speckle irradiance. The distance z was sufficiently long that the spatial structure of the speckle pattern was large compared to the width W of a single photosite on the detector array. In this low-frequency region, the MTF of the detector array is well approximated by

$$\mathrm{MTF}(\xi)=\left|\frac{\sin(\pi\xi W)}{\pi\xi W}\right| . \tag{8}$$

The measured PSD of the speckle irradiance is proportional to the square of the MTF in Eq. (8), and thus the actual PSD of the holographically reconstructed speckle is calculated by dividing the measured PSD by the square of the MTF in Eq. (8).

The theoretical PSD is constant over the range from 5 to 8.5 cycles/mm for the value of z used. The measured speckle PSD and the theoretical PSD are compared in Fig. 6, where the measured PSD has been corrected by the sinc^2 factor

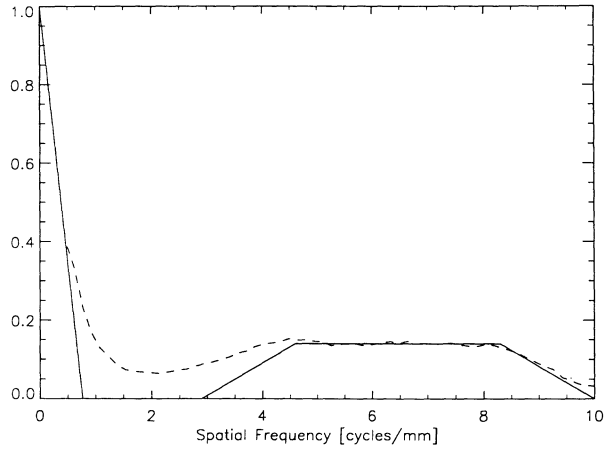

Fig. 6 PSD of irradiance for slant-slit aperture: theoretical (solid line) and measured (dashed line).

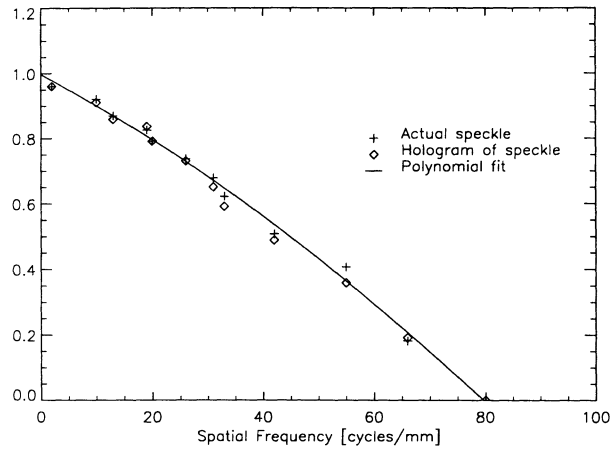

Fig. 7 Measured MTF of Pulnix camera.

mentioned previously. The MTF of the instrument does not affect the PSD of the speckle pattern in the flat region. Because the speckle pattern for higher spatial frequencies (small z) is simply a scaled representation of the pattern at low spatial frequencies (large z), it follows that the MTF of the instrument is equal to one for all frequencies needed to test the MTF of a detector array.

6 MTF of CCD Focal-Plane Array

We compare the MTFs of a CCD focal-plane array measured using the method of Ref. 1 and measured using the holographic element. A Pulnix 7CN focal-plane array was first tested using an integrating sphere and a two-slit aperture. Speckle patterns were recorded at nine different spatial frequencies. The processed data are plotted in Fig. 7 as "actual speckle." Next, the hologram of the two-slit laser speckle was used in the playback system with the Pulnix 7CN camera. Speckle patterns were recorded at the same nine spatial frequencies and processed in exactly the same way as the "actual speckle."

The "actual speckle" data are fitted with a third-order polynomial to show the trend of the complete MTF curve. The rms error between the "actual speckle" and "hologram of speckle" data was calculated to be 2%.

7 Conclusions

We have shown that using a hologram to produce narrowband laser speckle is a viable technique for testing the MTF of detector arrays. The input laser-power requirement was reduced by a factor of 100, making the speckle MTF method usable for a wider range of low-power lasers.

Acknowledgment

This work was supported by U.S. Air Force Wright Laboratory, Eglin AFB, Florida, under contract DAAB07-88-C-F405.

References

1. M. Sensiper, G. Boreman, A. Ducharme, and D. Snyder, "Modulation transfer function testing of detector arrays using narrow-band laser speckle," *Opt. Eng.* **32**(2), 395–400 (1993).
2. G. Boreman, Y. Sun, and A. James, "Generation of laser speckle with an integrating sphere," *Opt. Eng.* **29,** 339–342 (1990).
3. D. Goebel, "Generalized integrating-sphere theory," *Appl. Opt.* **6**(1), 125–128 (1967).
4. A. Fimia, A. Beléndez, and I. Pacual, "Influence of R-10 bleaching on latent image formation in silver halide-sensitized gelatin," *Appl. Opt.* **31**(17), 3203–3205 (1992).
5. J. Goodman, *Introduction to Fourier Optics,* McGraw-Hill, New York, 1968, pp. 244–246.

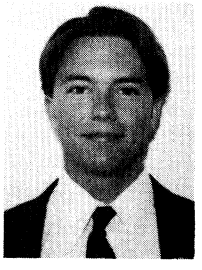

Alfred D. Ducharme received the BSEE degree from the University of Lowell, now known as the University of Massachusetts at Lowell, in 1990, and the MSEE and PhD degrees from the University of Central Florida, Center for Research and Education in Optics and Lasers, in 1992, and 1994, respectively. He is now a member of the technical staff at Physical Sciences Inc., Andover, Massachusetts.

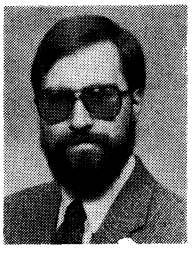

Glenn D. Boreman is an associate professor of electrical engineering in the Center for Research and Education in Optics and Lasers (CREOL) at the University of Central Florida. He received a BS from the Institute of Optics, University of Rochester, and a PhD from the Optical Sciences Center, University of Arizona. He has held visiting research positions at IT&T, Texas Instruments, U.S. Army Night Vision Lab, and McDonnell Douglas, and spent a sabbatical with the Applied Optics Group of Imperial College, London. Dr. Boreman serves as topical editor for *Applied Optics* in the areas of radiometry and detectors. He is the author of the MTF chapter in the second edition of the *Handbook of Optics,* as well as coauthor of the book, "Infrared Detectors and Systems" (John Wiley and Sons). He has published more than 60 articles in various aspects of optics including: infrared-detector and focal-plane analysis, adaptive optics, radiometry, laser speckle, and transfer-function techniques.